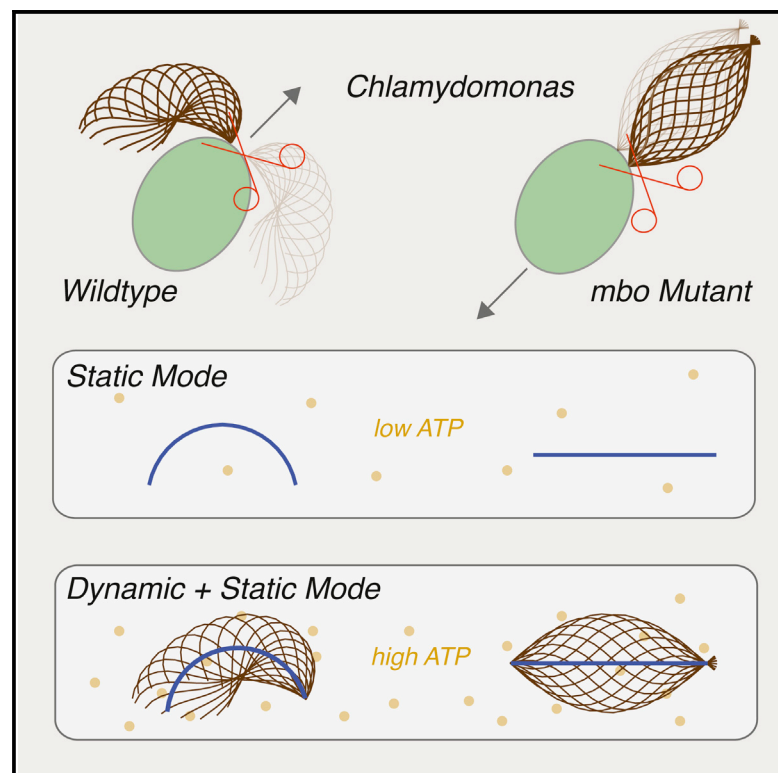


Current Biology

Independent Control of the Static and Dynamic Components of the *Chlamydomonas* Flagellar Beat

Graphical Abstract



Authors

Veikko F. Geyer, Pablo Sartori,
Benjamin M. Friedrich, Frank Jülicher,
Jonathon Howard

Correspondence

jonathon.howard@yale.edu

In Brief

The motility of the green alga *Chlamydomonas* is achieved by the beat of their two flagella. Geyer et al. show that the flagellar beat comprises a dynamic wave that travels around a static circular shape. Independent control of the two components allows cells to separately change propulsion and direction, through different molecular mechanisms.

Highlights

- The dynamic component is a traveling wave that provides propulsion
- The static component is a circular arc that controls direction
- The two components require ATP but differ in their ATP concentration dependences
- Mutations show that either component can exist in the absence of the other



Independent Control of the Static and Dynamic Components of the *Chlamydomonas* Flagellar Beat

Veikko F. Geyer,¹ Pablo Sartori,² Benjamin M. Friedrich,² Frank Jülicher,² and Jonathon Howard^{1,*}

¹Department of Molecular Biophysics and Biochemistry, Yale University, New Haven, CT 06511, USA

²Max Planck Institute for the Physics of Complex Systems, Dresden 01187, Germany

*Correspondence: jonathon.howard@yale.edu

<http://dx.doi.org/10.1016/j.cub.2016.02.053>

SUMMARY

When the green alga *Chlamydomonas reinhardtii* swims, it uses the breaststroke beat of its two flagella to pull itself forward [1]. The flagellar waveform can be decomposed into a static component, corresponding to an asymmetric time-averaged shape, and a dynamic component, corresponding to the time-varying wave [2]. Extreme lightening conditions photoshock the cell, converting the breaststroke beat into a symmetric sperm-like beat, which causes a reversal of the direction of swimming [3]. Waveform conversion is achieved by a reduction in magnitude of the static component, whereas the dynamic component remains unchanged [2]. The coupling between static and dynamic components, however, is poorly understood, and it is not known whether the static component requires the dynamic component or whether it can exist independently. We used isolated and reactivated axonemes [4] to investigate the relation between the two beat components. We discovered that, when reactivated in the presence of low ATP concentrations, axonemes displayed the static beat component in absence of the dynamic component. Furthermore, we found that the amplitudes of the two components depend on ATP in qualitatively different ways. These results show that the decomposition into static and dynamic components is not just a mathematical concept but that the two components can independently control different aspects of cell motility: the static component controls swimming direction, whereas the dynamic component provides propulsion.

RESULTS

To investigate the coupling of the static and the dynamic components of the *Chlamydomonas* beat, we examined the effect of ATP on the waveforms of isolated, demembrated, and reactivated axonemes [4–6] of *Chlamydomonas* wild-type (WT) cells and mutant cells that move backward only (*mbo2*) [7] (Figures 1A and 1H). The experimental methods for cell growth, deflagellation by the dibucaine procedure, and ATP reactivation are detailed in [8] and the Supplemental Information.

Measurement of the Waveforms of Beating Axonemes

The waveforms of beating axonemes were measured using high-speed video phase-contrast microscopy at 1,000 frames per second. Sequential images of a typical axoneme reactivated with 1 mM ATP are shown in Figures 1B (WT) and 1I (*mbo2*). In each frame, we traced the centerlines of the axonemes using tracking software [9]. The proximal end was defined as the end pointing in the swimming direction, which was always clockwise for axonemes observed on the lower chamber surface. The proximal end corresponds to the base of the flagellum and is where wave propagation starts [10]. The resulting shapes are plotted at 1-ms intervals over one beat cycle in Figure 1C. Visually, the series of shapes resembles those adopted by intact flagella undergoing normal breaststroke motility (Figure 1A) [10–12].

Mathematical Separation of the Waveform into Static and Dynamic Components

To quantify the key geometric properties of the waveform, we used an angular representation (Figure 1D), in which the tangent angle ψ with respect to the laboratory coordinate system is plotted for each point on the arc length of the axoneme and at each point in time (frame) in the movie (see also [10, 11, 13, 14]).

We define the static component of the waveform as the average angle over one beat cycle at each position along the axoneme (red line in Figure 1D). The mean angle decreases approximately linearly with arc length, corresponding to an approximately circular shape (shown as the red line in Figure 1C). We parameterized this static circular arc by its curvature $C = \psi_0/L$, where ψ_0 is the difference in tangent angle between the distal and proximal ends and L is the length of the axoneme (Figure 1D). To isolate the dynamic component, we subtracted the static mean shape from Figure 1D to obtain Figure 1E. The corresponding x - y representation is shown in Figure 1F. Note that both the angular and x - y representations are now symmetric. The dynamic component of the waveform can be approximated by a traveling wave of amplitude A , wavelength λ , and frequency f , defined in Figures 1E and 1G and the Supplemental Information, Figures S1, and S2. The mean values of the shape parameters summarize the key geometric properties of the waveform, which are presented in Table 1 (column 2 for WT axonemes).

To show that the dynamic component can exist in the absence of the static component, we repeated the waveform quantification for axonemes isolated from *mbo2* cells. A representative example is presented in Figures 1H–1N. The waveforms of *mbo2* axonemes resemble those of intact flagella from photoshocked cells, which is reflected in the similarity of the shape parameters (compare Table 1, columns 3 and 5). The static component of

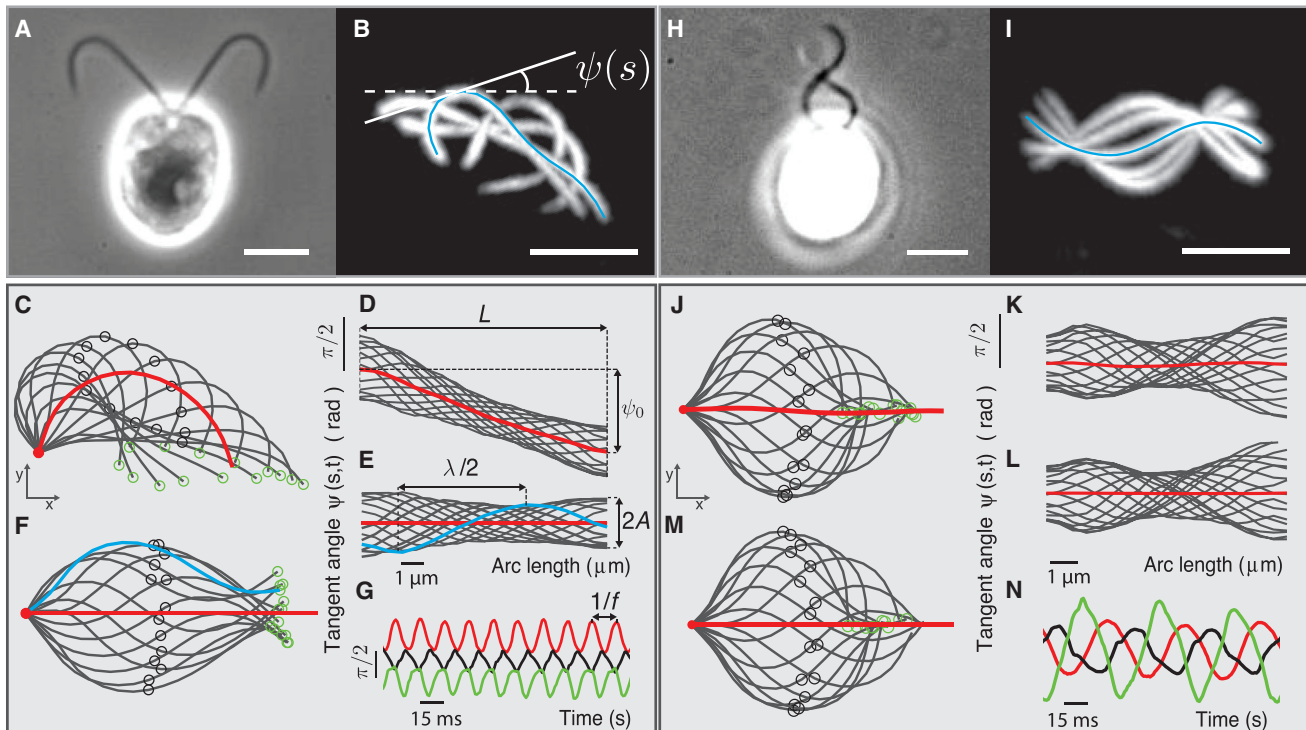


Figure 1. Characterization of the Breaststroke Beat of Isolated *Chlamydomonas* Axonemes

(A) A wild-type cell imaged using phase-contrast microscopy with an exposure time of 1 ms. The scale bar represents 5 μm .

(B) An axoneme isolated from a WT cell was imaged using phase-contrast microscopy with an exposure time of 1 ms. Four sequential contrast-inverted images were superimposed ($\Delta t = 3$ ms). The tangent angle $\psi(s, t)$ was measured with respect to the coordinate frame of the lab (gray dashed arrows). Note that the isolated axonemes swim in a circle.

(C) Tracked x - y shapes with subtracted rotation are represented for one beat cycle ($\Delta t = 1$ ms between curves). The colored open circles depict the basal end (red), the midpoint (black), and distal tip (green) corresponding to (G). The red curve presents the time-averaged shape.

(D) The tangent angles are plotted as a function of arc length $\psi(s, t_0)$ for the curves shown in (C). The red curve corresponds to the red shape highlighted in (C), which is the angular representation of the mean shape. The slope of the red curve corresponds to the mean curvature C calculated as $C = \psi_0/L$.

(E) Tangent angles after subtraction of the mean shape: this is the dynamic component. The blue curve was used to determine the wavelength λ , defined as two times the distance between the minimum and the maximum angle. The wave amplitude A was defined as the half-width of the waveform envelope averaged over the arc length.

(F) Shapes of the dynamic component shown in Figure 1F. Note that the mean shape of this waveform is a straight line (red curve).

(G) Tangent angle at a fixed arc length, s , as a function of time, $\psi(s_0, t)$, for the base ($s_0 = 0$, orange), midpoint ($s_0 = L/2$, black), and distal tip ($s_0 = L$, green). The beat frequency f is given by the inverse of the time between peaks. See Figure S1 for more detailed information on the shape parameterization.

(H–N) Equivalent to (A)–(G) for the *mbo2* mutant. Reactivated *mbo2* axonemes were imaged using dark-field microscopy.

the *mbo2* waveform is very small: the red lines in Figures 1J and 1K are almost straight. On the other hand, the dynamic components of mutant and WT axonemes are very similar (compare Figure 1E to Figure 1L and Figure 1F to Figures 1J and 1M).







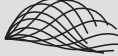
In summary, our analysis shows that the static and dynamic components of the beat can be separated geometrically and that the dynamic component can exist in absence of the static component as observed for *mbo2* axonemes and photoshocked cells (see Table 1). In both cases, the dynamic components of the beats are very similar. This generalizes an earlier result in intact cells showing that the primary effect of photoshock is to abolish the static component of the beat [2].

The Breaststroke Is a Sinusoidal Waveform Traveling around a Circular Arc

Our decomposition of the axonemal beat into static and dynamic components suggests that the breaststroke beat can be viewed

as a sinusoidal, sperm-like waveform traveling around a static, circular arc. In the absence of the static component (Figure 2A, upper panel), the x - y waveform is sperm-like (Figure 2A, lower). When a static component with a constantly decreasing angle (Figure 2B, upper), corresponding to a circular arc (Figure 2B, lower), is added to the dynamic mode (Figure 2A, upper), the resulting waveform becomes asymmetric (Figure 2C, upper) and resembles the breaststroke beat of WT axonemes (Figure 2C, lower). The model waveform Figure 2C captures the effective and recovery phases of the breaststroke. During the effective phase of the beat, the dynamic component has opposite curvature to that of the mean curvature. This leads to a partial cancellation of the static curvature and a straightening of the axoneme. When the flagellum is attached to the cell, the effective stroke powers forward motion. During the recovery phase of the beat, the dynamic component has the same curvature to that of the static component. The summation increases the curvature and

Table 1. Shape Parameters and Corresponding Shapes for the Simplified Waveform Model

Strain	WT Axoneme ^a	<i>mbo2</i> Axoneme ^a	<i>uni1</i> Cell ^b	<i>uni1</i> Cell (PS) ^b	<i>oda1</i> Cell (<i>oda38</i>) ^b	<i>ida1/4</i> Cell (<i>ida98</i>) ^b	<i>pf2</i> Cell ^b
Curvature <i>C</i> (rad/μm)	-0.24 ± 0.02	-0.04 ± 0.01	-0.17 ± 0.005	-0.01 ± 0.05	-0.16 ± 0.04	-0.19 ± 0.06	-0.1 ± 0.07
Amplitude <i>A</i> (rad)	0.68 ± 0.04	0.90 ± 0.08	1.08 ± 0.09	1.13 ± 0.07	0.98 ± 0.09	0.78 ± 0.07	0.64 ± 0.17
Wavelength λ (μm)	11.4 ± 0.7	11.0 ± 0.6	15.1 ± 2.0	12.6 ± 1.4	18.7 ± 2.9	11.6 ± 1.7	14.8 ± 4.1
Length <i>L</i> (μm)	11.7 ± 0.4	9.2 ± 0.3	12.8 ± 1.5	12.7 ± 1.7	11.6 ± 1.2	10.4 ± 1.2	12.5 ± 1.4
Frequency <i>f</i> (Hz)	68 ± 3	28 ± 7	63 ± 6	73 ± 8	25 ± 4	55 ± 7	51 ± 18
Waveform ^c							

^aData from this study: reactivated axonemes at 24°C using 1 mM ATP (mean ± SD; n = 6).

^bData from Tables 1, 2, and 3 of [10] were converted to the simplified waveform model using the equations provided in the Supplemental Information. Mean ± SD (SD is calculated by propagating errors). The parameters for *uni* cells from [10] agree with values obtained by direct measurements (see Table S1).

^cThe waveforms were reconstructed from the mean shape parameters using the equation in the caption of Figure 2, explained in the Supplemental Information.

leads to a highly bent flagellum. This results in a small reversal of cell motion during the recovery stroke [12, 17, 18]. Thus, the combination of static and dynamic components account for the main features of the breaststroke beat.

ATP Titration Separates the Static Component from the Dynamic Component

To test whether the static component of the beat can also exist in the absence of the dynamic component, we measured axonemal shapes over a large range of ATP concentrations (Figure 3). When the ATP concentration was gradually decreased from 1 mM to 50 μM, the static curvature of the static component was unaffected (Figure 3A). The amplitude of the dynamic component remained unchanged (Figure 3B), though the frequency decreased (Figure 3C). However, when the ATP concentration was decreased below 50 μM, the axonemes ceased to beat, as the dynamic component vanished (Figures 3C and 3D). We quantified this response to ATP by fitting a Hill equation to the data (see figure caption of Figure 3). The Hill coefficient, *n*, is usually associated with cooperative binding of a ligand or the nonlinear activation of an enzyme, and the *K_m* value typically corresponds to the ligand concentration at half-maximal enzyme activity [19]. We found that the transition from beating to non-beating was abrupt, occurring over a narrow range of ATP concentrations centered at 47 μM. An abrupt decrease in amplitude was also observed for *mbo2*, at an ATP concentration between 60 and 90 μM. The abrupt decrease in amplitude indicates that the underlying process is highly cooperative (Hill coefficient *n* = 52 for WT and *n* = 59 for *mbo2*; Figure 3B). In the theory of dynamical systems, an abrupt change of oscillation amplitude as a function of a control parameter is a feature of a subcritical Hopf bifurcation [20]. Thus, the dynamic component has the signature of a collective phenomenon [21].

In contrast to the dynamic component, the mean curvature of the static component decreased gradually as the ATP concentration was decreased. There was no evidence for cooperativity (the Hill coefficient was not significantly different from 1; Figure 3A). The ATP concentration necessary for half-maximal amplitude was 17 μM. Importantly, at ATP concentrations below

47 μM, the non-beating WT axonemes still displayed a static component with high curvature (Figure 3A). An example of such a static shape is shown in Figure 3D (upper panel). In the absence of ATP, the axonemes were straight with zero curvature (Figure 3D, middle panel). The dependence of the static curvature on the ATP concentration indicates that it is sustained by an active process. Consistent with this conclusion, the static curvature was greatly reduced by addition of the ATPase inhibitor vanadate (Figures 3A–3C, black open diamonds), which also inhibits axonemal dyneins [22]. Note that, in *mbo2* axonemes, the static component is close to zero at all ATP concentrations. The different ATP dependencies of the static and dynamic components show that there is no obligate coupling between the two components: each can exist in the absence of the other.

Waveforms with Any Combination of Static and/or Dynamic Component Are Observed

To illustrate the full range of static and dynamic components that can be observed, we plotted both components for WT and *mbo2* axonemes in a state diagram (Figure 3E). The static component is represented by its mean curvature and the dynamic component by its amplitude. The data populate all quadrants of the diagram: (1) straight and non-beating axonemes (no ATP); (2) bent and non-beating axonemes (WT; low ATP); (3) bent and beating axonemes (WT; high ATP); and (4) straight and beating axonemes (*mbo2*; high ATP). In addition to the WT and *mbo2* axonemes (data from Figures 3A–3C), we have added data from the intact flagella of *uni1* mutants, a strain that has only a single flagellum [10], which has large static and dynamic components (3); the intact flagella of *pf18oda1* mutants [23], which are immotile (no dynamic component) but have large mean curvatures (large static component) (2); and the intact flagella of photoshocked *uni1* cells, which have large dynamic components but only small mean curvatures (4) [10] and are similar to isolated axonemes in high calcium [5, 24]. Thus, all combinations of static and dynamic components are possible. This adds further support to the notion that the static and dynamic components are independently determined in the cell.

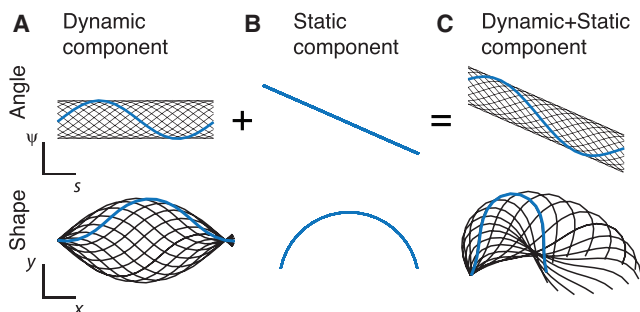


Figure 2. Model of the Breaststroke Beat as a Sinusoidal Waveform Traveling around a Circular Arc

(A) The dynamic component comprises a traveling wave with constant amplitude: $\psi_D(s, t) = A \sin(2\pi(ft + s/\lambda))$; see also Figure S2. The upper panel shows the angular representation. The lower panel shows the x - y shapes given by $x(s) = x_0 + \int_0^s \cos \psi(s') ds'$ and $y(s) = y_0 + \int_0^s \sin \psi(s') ds'$ [14–16].

(B) A circular arc (lower) corresponds to a linear angle profile (upper). $\psi_S(s) = Cs$.

(C) When the dynamic component is superimposed on the circular arc by addition of the tangent angles $\psi_{D+S}(s, t) = Cs + A \sin(2\pi(ft + s/\lambda))$ (upper), the resultant x - y shape resembles a breaststroke (lower). The following parameter values were used: $C = -0.23$ rad/ μm ; $A = 0.73$ rad; $\lambda = 11.8$ μm ; $L = 11.1$ μm . These parameters correspond to the WT axoneme in Figure 1.

DISCUSSION

We have shown that the breaststroke beat of isolated *Chlamydomonas* axonemes can be well approximated by the superposition of dynamic and static components. This superposition corresponds to a symmetric, sperm-like beat traveling around a static circular arc. This extends earlier work by Eshel and Brokaw, who discussed the possibility of such a decomposition for the waveforms of normally beating and photoshocked *uni1* cells [2]. This finding emphasizes the close relationship between the breaststroke and sperm-like flagellar waveforms. Importantly, we found that the static and dynamic beat components can be independently controlled by changing the ATP concentration: this has important implications for the identification of the molecular mechanism underlying the static component, as well as its biological function.

Molecular Origin of the Static Component

The geometry of the static component together with its ATP dependence constrains models describing the underlying molecular mechanisms. Mutational studies show that outer arm dyneins and several inner arm dyneins (*a*, *c*, *d*, *e*, and *f*) are not required for the static component because the waveforms of these mutants are asymmetric [25, 26] (see Table 1 for examples). If a specific dynein is required for the static curvature, then it is likely to be one of the less well-studied inner arm dyneins. These include inner dynein arm *b* (DHC5); *g* (DHC7); and the minor inner arm dyneins [27] DHC3, DHC4, and DHC11. That inner arm dyneins induce the static curvature is consistent with the ATP requirements for in vitro motility of inner arm dyneins: their K_m values—10 μM for IDAb, 22 μM for IDAe, and 32 μM for IDAa [28]—are similar to the ATP requirement of the static curvature (17 μM). A possible scenario is the inner dynein arms create asymmetry and contribute to the dynamic component, whereas outer dynein arms only add to the dynamic component [29].

The geometry of the static component indicates that there is a spatial imbalance of force generation within the axoneme. To produce a static curvature with the correct sign, the sliding forces between doublet microtubules 2–6 must be larger than those produced in the opposing half of the axoneme, between doublets 6 and 9. Moreover, because the static shape is approximately circular, force generation must be concentrated toward the distal end of the axoneme [30]. Such radial and longitudinal localization of motor activity could be due to (1) appropriate localization of dynein or other force-generating elements, (2) appropriate localization of proteins that regulate uniformly distributed motors, or (3) a feedback control mechanism that restricts the activity of uniformly distributed motors and regulators. None of these three mechanisms can be ruled out. For example, there are dyneins that are distributed asymmetrically, both radially and longitudinally [27, 31], and there are also asymmetrically distributed regulators like the dynein regulatory complex (DRC) [32]. Finally, it has been shown that doublet curvature or normal forces, which separate doublets, can lead to longitudinal asymmetry of motor activity [14, 33, 34] and circular arcs [30]. Thus, the molecular mechanism underlying the static component remains unknown, though our results place constraints on possible mechanisms.

The Static Component Determines Swimming Speed and Direction of Swimming of Biflagellated Cells

Our work shows that the major difference between breaststroke waveforms, which in *Chlamydomonas* propel forward motion, and sperm-like waveforms, which propel backward motion, is the presence or absence of the static component, which makes the waveform asymmetric. Because the absence of mean curvature reverses the swimming direction, we predict that there is an intermediate curvature of the static component at which the swimming speed is zero. The *Chlamydomonas pf2* and *pf3* mutants, which have abnormal waveforms, exhibit a decreased mean curvature [25]. Consistent with our prediction, the swimming speeds of *pf2* and *pf3* are decreased to one-third and one-half the WT speeds, respectively [35]. Thus, modulation of the curvature of the static component may contribute to the swimming phenotypes of *Chlamydomonas* mutants. We note that other factors such as amplitude, frequency, and wavelength can also contribute to vary the swimming velocity.

In reactivation assays, it was shown that the static asymmetry can be modulated by calcium [4, 5], allowing study of the swimming behavior of cell models with different static asymmetries [36]. In these studies, it was found that, at intermediate calcium concentrations of (10^{-6}M), corresponding to an intermediate static asymmetry, 10% of the cells exhibited flagellar oscillations that produced no net movement. Again, this is consistent with our prediction. Thus, the static component can modulate the swimming speed and direction of biflagellated cells.

The static component also influences the direction of swimming in other organisms. Trypanosomatid flagella such as those of *Leishmania major*, which usually have a sperm-like beat, have been observed to undergo asymmetric breaststroke waveforms [37]. Because they have only one flagellum, this motion yaws the cell body (like the isolated WT *Chlamydomonas* axoneme), leading to reorientation of the cell. This may play a

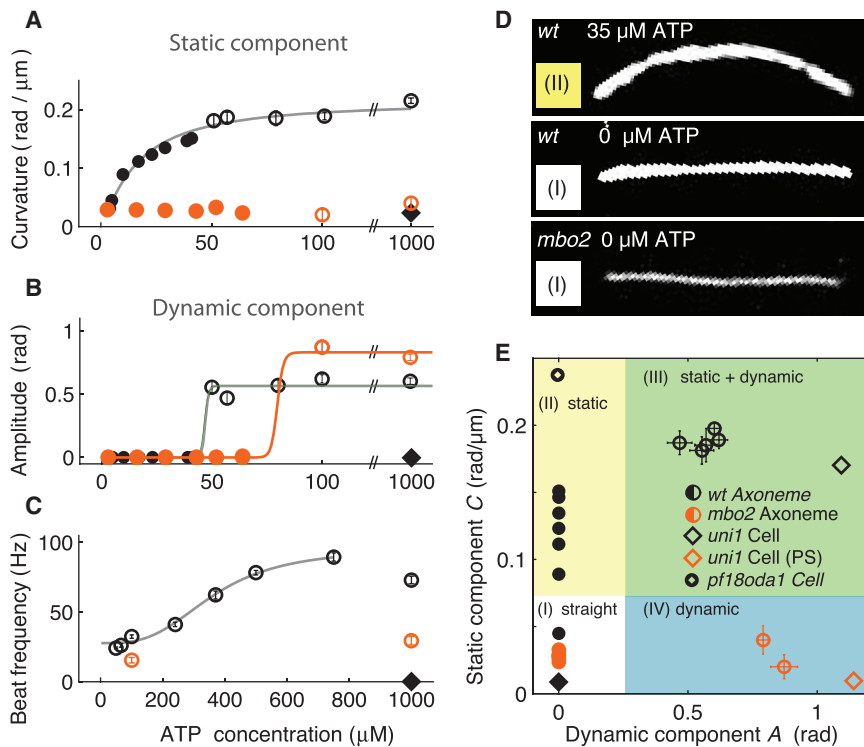


Figure 3. Experimental Separation of the Static and Dynamic Components of the Beat of WT and *mbo2* Axonemes at Different ATP Concentrations

(A) The static component (the mean curvature) as a function of ATP concentration. In all panels, the black circles depict WT and the orange circles *mbo2* axonemes; solid circles indicate non-motile axonemes and open circles motile ones. The filled diamond represents WT axonemes in 1 mM ATP + 80 μM vanadate. In all panels, the solid curves represent a fit of the Hill equation to the data $y = \max_y / (1 + (K_m/x)^n) - \min_y$. K_m is the ATP concentration at which half-maximum amplitude is reached. The Hill coefficient, n , corresponds to cooperativity. For the WT axonemes, $K_m = 17 \pm 5 \mu\text{M}$ and $n = 1.3 \pm 0.3$.

(B) The mean amplitude of the dynamic component as a function of ATP concentration. The parameters of Hill equation for WT axonemes is $K_m = 47 \pm 2 \mu\text{M}$ and $n = 52 \pm 17$. For *mbo2*, the parameters are $K_m = 80 \pm 8 \mu\text{M}$, $n = 59 \pm 19$.

(C) Beat frequency as function of ATP concentration. The parameters of the Hill equation for WT axonemes are $K_m = 361 \pm 19 \mu\text{M}$ and $n = 3.1 \pm 0.4$.

(D) Representative images of WT and *mbo2* axonemes. Upper: immotile WT axoneme at 35 μM ATP (inverted phase contrast). Middle: WT axoneme in the absence of ATP (inverted phase contrast). Lower: *mbo2* axoneme in the absence of ATP (dark-field microscopy).

(E) State diagram of shapes of reactivated axonemes in which the mean amplitude of the dynamic component is plotted on the x axis and the amplitude of the static component on the y axis.

role in obstacle avoidance. Thus, addition of a static component to the trypanosomatid beat leads to reorientation of the direction of swimming.

Spermatozoa use a related, though more-subtle, mechanism for controlling their swimming direction. The presence of a small mean curvature causes sperm to swim along shallow circular or helical paths [38], and the regulation of curvature is likely to be the key steering mechanism by which spermatozoa chemotax up chemical gradients [39, 40]. Thus, modulation of the magnitude of the static component is a general mechanism that flagellated cells use to direct their motility. The independence of the static and dynamic components allows direction and propulsion to be controlled separately.

SUPPLEMENTAL INFORMATION

Supplemental Information includes Supplemental Experimental Procedures, two figures, and one table and can be found with this article online at <http://dx.doi.org/10.1016/j.cub.2016.02.053>.

AUTHOR CONTRIBUTIONS

Conceptualization and Writing – Review & Editing, V.F.G., J.H., P.S., F.J., and B.M.F. Investigation, Methodology, Formal Analysis, and Writing – Original Draft, V.F.G.; Resources and Supervision, J.H.

ACKNOWLEDGMENTS

We thank Joshua Alper, Vikram Mukundan, and Sujoy Ganguly for helpful discussions and ongoing support during the project and Bill Shin and Joe Brzostowski for organizing the supply of latest camera technology to the Physiology

course in Woods Hole, MA. Finally, we appreciate all the insightful discussions and comments on the manuscript by the members of the J.H. lab. This work was supported by Yale University and the Max Planck Society.

Received: June 21, 2015

Revised: December 1, 2015

Accepted: February 19, 2016

Published: March 31, 2016

REFERENCES

- Ringo, D.L. (1967). Flagellar motion and fine structure of the flagellar apparatus in *Chlamydomonas*. *J. Cell Biol.* 33, 543–571.
- Eshel, D., and Brokaw, C.J. (1987). New evidence for a “biased baseline” mechanism for calcium-regulated asymmetry of flagellar bending. *Cell Motil. Cytoskeleton* 7, 160–168.
- Witman, G.B. (1993). *Chlamydomonas* phototaxis. *Trends Cell Biol.* 3, 403–408.
- Bessen, M., Fay, R.B., and Witman, G.B. (1980). Calcium control of waveform in isolated flagellar axonemes of *Chlamydomonas*. *J. Cell Biol.* 86, 446–455.
- Wakabayashi, K., Yagi, T., and Kamiya, R. (1997). Ca^{2+} -dependent waveform conversion in the flagellar axoneme of *Chlamydomonas* mutants lacking the central-pair/radial spoke system. *Cell Motil. Cytoskeleton* 38, 22–28.
- Frey, E., Brokaw, C.J., and Omoto, C.K. (1997). Reactivation at low ATP distinguishes among classes of paralyzed flagella mutants. *Cell Motil. Cytoskeleton* 38, 91–99.
- Segal, R.A.R., Huang, B., Ramanis, Z., and Luck, D.J.D. (1984). Mutant strains of *Chlamydomonas reinhardtii* that move backwards only. *J. Cell Biol.* 98, 2026–2034.

8. Alper, J., Geyer, V., Mukundan, V., and Howard, J. (2013). Reconstitution of flagellar sliding. *Methods Enzymol.* *524*, 343–369.
9. Ruhnaw, F., Zwicker, D., and Diez, S. (2011). Tracking single particles and elongated filaments with nanometer precision. *Biophys. J.* *100*, 2820–2828.
10. Brokaw, C.J., and Luck, D.J. (1983). Bending patterns of chlamydomonas flagella I. Wild-type bending patterns. *Cell Motil.* *3*, 131–150.
11. Bayly, P.V., Lewis, B.L., Kemp, P.S., Pless, R.B., and Dutcher, S.K. (2010). Efficient spatiotemporal analysis of the flagellar waveform of *Chlamydomonas reinhardtii*. *Cytoskeleton (Hoboken)* *67*, 56–69.
12. Geyer, V.F., Jülicher, F., Howard, J., and Friedrich, B.M. (2013). Cell-body rocking is a dominant mechanism for flagellar synchronization in a swimming alga. *Proc. Natl. Acad. Sci. USA* *110*, 18058–18063.
13. Gray, J., and Hancock, G.J. (1955). The propulsion of sea-urchin spermatozoa. *J. Exp. Biol.* *32*, 802–814.
14. Riedel-Kruse, I.H., Hilfinger, A., Howard, J., and Jülicher, F. (2007). How molecular motors shape the flagellar beat. *HFSP J.* *1*, 192–208.
15. Hines, M., and Blum, J.J. (1978). Bend propagation in flagella. I. Derivation of equations of motion and their simulation. *Biophys. J.* *23*, 41–57.
16. Bayly, P.V., Lewis, B.L., Ranz, E.C., Okamoto, R.J., Pless, R.B., and Dutcher, S.K. (2011). Propulsive forces on the flagellum during locomotion of *Chlamydomonas reinhardtii*. *Biophys. J.* *100*, 2716–2725.
17. Racey, T.J., Hallett, R., and Nickel, B. (1981). A quasi-elastic light scattering and cinematographic investigation of motile *Chlamydomonas reinhardtii*. *Biophys. J.* *35*, 557–571.
18. Kamiya, R. (2000). Analysis of cell vibration for assessing axonemal motility in *Chlamydomonas*. *Methods* *22*, 383–387.
19. Hill, A.V. (1910). The possible effects of the aggregation of the molecules of haemoglobin on its dissociation curves. *J. Physiol.* *40*, i–vii.
20. Strogatz, S.H. (2014). *Nonlinear Dynamics and Chaos* (Westview Press).
21. Brokaw, C.J. (2009). Thinking about flagellar oscillation. *Cell Motil. Cytoskeleton* *66*, 425–436.
22. Oda, T., Hirokawa, N., and Kikkawa, M. (2007). Three-dimensional structures of the flagellar dynein-microtubule complex by cryoelectron microscopy. *J. Cell Biol.* *177*, 243–252.
23. Hayashibe, K., Shingyoji, C., and Kamiya, R. (1997). Induction of temporary beating in paralyzed flagella of *Chlamydomonas* mutants by application of external force. *Cell Motil. Cytoskeleton* *37*, 232–239.
24. Omoto, C.K., and Brokaw, C.J. (1985). Bending patterns of *Chlamydomonas flagella*: II. Calcium effects on reactivated *Chlamydomonas flagella*. *Cell Motil.* *5*, 53–60.
25. Brokaw, C.J., and Kamiya, R. (1987). Bending patterns of *Chlamydomonas flagella*: IV. Mutants with defects in inner and outer dynein arms indicate differences in dynein arm function. *Cell Motil. Cytoskeleton* *8*, 68–75.
26. Witman, G. (2009). *The Chlamydomonas Sourcebook: Cell Motility and Behavior* (Academic Press).
27. Yagi, T., Uematsu, K., Liu, Z., and Kamiya, R. (2009). Identification of dyneins that localize exclusively to the proximal portion of *Chlamydomonas flagella*. *J. Cell Sci.* *122*, 1306–1314.
28. Kagami, O., and Kamiya, R. (1992). Translocation and rotation of microtubules caused by multiple species of *Chlamydomonas* inner-arm dynein. *J. Cell Sci.* *103*, 653–664.
29. Kamiya, R., and Okamoto, M. (1985). A mutant of *Chlamydomonas reinhardtii* that lacks the flagellar outer dynein arm but can swim. *J. Cell Sci.* *74*, 181–191.
30. Mukundan, V., Sartori, P., Geyer, V.F., Jülicher, F., and Howard, J. (2014). Motor regulation results in distal forces that bend partially disintegrated *Chlamydomonas* axonemes into circular arcs. *Biophys. J.* *106*, 2434–2442.
31. Bui, K.H., Yagi, T., Yamamoto, R., Kamiya, R., and Ishikawa, T. (2012). Polarity and asymmetry in the arrangement of dynein and related structures in the *Chlamydomonas* axoneme. *J. Cell Biol.* *198*, 913–925.
32. Bower, R., Tritschler, D., Vanderwaal, K., Perrone, C.A., Mueller, J., Fox, L., Sale, W.S., and Porter, M.E. (2013). The N-DRC forms a conserved biochemical complex that maintains outer doublet alignment and limits microtubule sliding in motile axonemes. *Mol. Biol. Cell* *24*, 1134–1152.
33. Lindemann, C.B. (1994). A “geometric clutch” hypothesis to explain oscillations of the axoneme of cilia and flagella. *J. Theor. Biol.* *168*, 175–189.
34. Lindemann, C.B. (2002). Geometric Clutch model version 3: the role of the inner and outer arm dyneins in the ciliary beat. *Cell Motil. Cytoskeleton* *52*, 242–254.
35. Gardner, L.C., O’Toole, E., Perrone, C.A., Giddings, T., and Porter, M.E. (1994). Components of a “dynein regulatory complex” are located at the junction between the radial spokes and the dynein arms in *Chlamydomonas flagella*. *J. Cell Biol.* *127*, 1311–1325.
36. Schmidt, J.A., and Eckert, R. (1976). Calcium couples flagellar reversal to photostimulation in *Chlamydomonas reinhardtii*. *Nature* *262*, 713–715.
37. Gadelha, C., Wickstead, B., and Gull, K. (2007). Flagellar and ciliary beating in trypanosome motility. *Cell Motil. Cytoskeleton* *64*, 629–643.
38. Ishijima, S., and Hamaguchi, Y. (1993). Calcium ion regulation of chirality of beating flagellum of reactivated sea urchin spermatozoa. *Biophys. J.* *65*, 1445–1448.
39. Crenshaw, H.C. (1996). A new look at locomotion in microorganisms: rotating and translating. *Am. Zool.* *36*, 608–618.
40. Kaupp, U.B., Kashikar, N.D., and Weyand, I. (2008). Mechanisms of sperm chemotaxis. *Annu. Rev. Physiol.* *70*, 93–117.